

Data Integration with Fusion Searchlight: Classifying Brain States from Resting-state fMRI

Simon Wein¹, Marco Riebel¹, Lisa-Marie Brunner¹, Caroline Nothdurfter¹, Rainer Rupprecht¹, and Jens V. Schwarzbach¹

¹Department of Psychiatry and Psychotherapy, University of Regensburg, Regensburg, Germany

Abstract

Spontaneous neural activity observed in resting-state fMRI is characterized by complex spatio-temporal dynamics. Different measures related to local and global brain connectivity and fluctuations in low-frequency amplitudes can quantify individual aspects of these neural dynamics. Even though such measures are derived from the same functional signals, they are often evaluated separately, neglecting their interrelations and potentially reducing the analysis sensitivity. In our study, we present a fusion searchlight (FuSL) framework to combine the complementary information contained in different resting-state fMRI metrics and demonstrate how this can improve the decoding of brain states. Moreover, we show how explainable AI allows us to reconstruct the differential impact of each metric on the decoding, which additionally increases spatial specificity of searchlight analysis. In general, this framework can be adapted to combine information derived from different imaging modalities or experimental conditions, offering a versatile and interpretable tool for data fusion in neuroimaging.

1 Introduction

Resting-state fMRI (rs-fMRI) studies intrinsic neural activity of the brain at rest and is characterized by complex spatial and temporal dynamics (Biswal et al., 1995). Until now, numerous methods have been established to describe and analyze different aspects of these spontaneous neural dynamics. Functional connectivity (FC) is a popular approach for studying global interactions between brain regions from a functional network perspective (van den Heuvel and Hulshoff Pol, 2010). Measures from graph theory allow us thereby to detect changes in connectivity properties of brain networks (Bassett and Sporns, 2017). On a smaller scale, regional homogeneity (ReHo) quantifies local connectivity across the cortex in the range of millimeters, and is defined as the temporal coherence or synchrony of the BOLD signal of neighboring voxels or vertices (Jiang and Zuo, 2016). In addition to connectivity measures, the fractional amplitude of low frequency fluctuations (fALFF) can characterize local modulations in the amplitude of signals (Yang et al., 2007; Zou et al., 2008). This quantity reflects the ratio of the BOLD signal's power spectrum of low frequencies to the signal's entire frequency range. In this manner, these different rs-fMRI metrics capture complementary aspects of BOLD signal dynamics (Lv et al., 2018). In clinical MRI studies for instance, changes in neural dynamics can be reflected simultaneously in multiple metrics. In rs-fMRI studies on depression, alterations have been linked to modulations in FC (Javaheripour et al., 2021; Kaiser et al., 2015), fALFF (Gao et al., 2021; Wang et al., 2022) and ReHo (Shen et al., 2017; Ni et al., 2023; Sun et al., 2022). Also multiple sclerosis has shown to affect a multitude of markers, such as FC (Tahedi et al., 2018; Huang

et al., 2020; Tahedi et al., 2022), fALFF (Liu et al., 2015) and ReHo (Wu et al., 2016). Furthermore, in a pharmacological rs-fMRI study, the sedative effects of alprazolam were observed simultaneously in the modulations of FC, ReHo and fALFF (Wein et al., 2024). However, many current rs-fMRI studies focus only on a single metric, or analyze these biomarkers separately. In this manner, information on important modulations of the BOLD signal may be neglected, potentially reducing sensitivity of detecting altered brain states¹.

In our study we present an interpretable framework based on searchlight (SL) decoding for fusing such complementary fMRI markers and improving analysis sensitivity. SL decoding uses multivariate pattern analysis (MVPA) to test the information content in small spherical subsets in every voxel or vertex across the cortex (Kriegeskorte et al., 2006; Etzel et al., 2013). In this manner SL typically produces spatial maps of decoding accuracies, highlighting areas that are informative for a specific brain state. In our fusion SL (FuSL) framework we integrate the distinct information of BOLD dynamics expressed in local ReHo, fALFF and global FC and show how this increases decoding performance in rs-fMRI. In a next step we utilize an explainable AI (XAI) approach to retrospectively trace back the feature importance of each metric for decoding. To this aim, we rely on Shapley additive explanations (SHAP) (Lundberg and Lee, 2017), a model-agnostic XAI method based on game theoretically optimal Shapley values (Shapley, 1953). Moreover, we show that incorporating XAI to evaluate feature importance has the additional benefit of increasing spatial specificity in SL analysis. Solely analyzing prediction accuracy, as typically done in current studies applying SL decoding, only reveals if there is somewhere within the SL radius information present. Thus, maps of decoding accuracies do not exactly represent maps of informative voxels (Etzel et al., 2013). Incorporating SHAP as a post hoc test can help us to reconstruct the precise locations of voxels within a SL that are most important for decoding, what helps us to increase spatial specificity of SL analysis.

We first investigate general properties the FuSL framework employing an artificial MRI dataset and study how different combinations of informative and uninformative data sources affect its decoding performance. With rs-fMRI data from a pharmacological fMRI study we further demonstrate that the integration of complementary rs-fMRI metrics can enhance the prediction of pharmacological treatment of participants. Sedative effects of benzodiazepines have shown to be reliably expressed in different rs-fMRI markers, such as FC (Wei et al., 2013; Hashmi et al., 2017; Schrouff et al., 2011), ReHo (Blanco-Hinojo et al., 2021) and fALFF (Kiviniemi et al., 2003, 2005). We show how combining these metrics can help us to detect sedation-related alterations in the BOLD signal, based on rs-fMRI data from participants who received either a benzodiazepine (alprazolam) or a placebo during a pharmacological study (Wein et al., 2024). We finally demonstrate how SHAP can be used to trace back the differential impact of sedation on the individual fMRI markers.

Numerous data fusion frameworks have meanwhile shown to be beneficial in diverse areas of neuroimaging analyses. In clinical neuroscience integrating distinct modalities such as functional MRI, structural MRI, EEG and MEG has improved our understanding on mental disorders (Calhoun and Sui, 2016). Fusing MEG or EEG with fMRI data using representational similarity analysis (RSA) allows characterizing neural activation simultaneously with high temporal and spatial resolution in cognitive neuroscience (Cichy et al., 2016; Cichy and Oliva, 2020). In brain connectivity research adding structural information to functional MRI data has helped adding biological constraints to computational and machine learning models of neural dynamics (Cabral et al., 2014; Suárez et al., 2020; Wein et al., 2021b,a). Merging information expressed in different structural MRI modalities has enhanced accuracy of segmenting tumors (Ahamed et al., 2023) and multiple sclerosis lesions (Zeng et al., 2020). In this study we demonstrate that data fusion can be also beneficial for SL decoding analysis. Besides improving decoding in rs-fMRI, our FuSL framework can be easily adapted to integrate information from different

¹Based on the definition of Greene et al. (2023), we refer as brain states to recurring activity patterns distributed across the brain that emerge from physiological or cognitive processes.

imaging modalities. While deep learning frameworks often require a large amount of training data and manual fine-tuning of model parameters (Schulz et al., 2020), SL has proven to be a robust and widely-used MVPA tool that limits its complexity inherently by using spatially localized information. Furthermore, using a model-agnostic feature attribution method based on Shapley values allows one to use a wide range of MVPA models for decoding in our workflow. In this manner our FuSL framework can provide a flexible and interpretable framework for diverse data fusion applications in neuroimaging.

2 Methods and Materials

2.1 Fusion searchlight

In our FuSL framework we integrate the complementary information provided by different data sources in a searchlight-based decoding analysis. For decoding a brain state based on resting-state fMRI we first computed regional homogeneity (ReHo), fractional amplitude of low frequency fluctuations (fALFF) and regional functional connectivity efficiency (FCE), and concatenated these values within each SL to train a classifier (figure 1 A and B). After training and testing the SL classifier using stratified cross validation (CV) (Kohavi, 1995), we obtained a spatial map of test accuracies across the cortex, pointing out vertices with neighborhoods that were informative to decode a specific brain state, like in classical SL analysis (figure 1 (C)). To identify test accuracies that were significantly different from chance level we permuted the labels and applied threshold-free cluster enhancement (TFCE) to the original and permuted accuracy maps (Smith and Nichols, 2009). To correct for multiple comparisons across vertices we took the maximum TFCE values of accuracy maps derived from permuted data to build the null distribution and tested the values of the original TFCE map against them (Smith and Nichols, 2009).

In a next step we aimed to explain the predictions of the FuSL classifier. To reveal which metrics had driven the decision of the SL, we used Shapley additive explanations (SHAP) to reconstruct the importance of each metric at each location on the cortex (Lundberg and Lee, 2017). This explanation approach assigns post-hoc an importance score to each input feature of a classifier, which we utilized to determine whether modulations in ReHo, fALFF or FCE were indicative for decoding a specific brain state. For each SL we first computed the feature importance of each metric at each vertex and then averaged these values across overlapping SLs at each vertex. In this manner we obtained one importance score for each metric at each vertex on the cortex. A formal derivation of these importance measure is provided in Supplement I. To obtain maps that reflect simultaneously the *importance* and the *informativeness* of a metric, we further weighted spatial maps of SHAP values (feature importance) with the spatial map of decoding accuracies (informativeness). We denoted this combination of informativeness and importance as the actual *impact* of a metric (figure 1 (D)). However, these maps do not provide us with information whether a metric is increased or decreased due to an intervention or condition, which can be valuable information for the interpretation of analysis results. To address this shortcoming we propose to additionally incorporate a third characteristic of the data. We computed the differences in metrics between the groups across the cortex to obtain a spatial map indicating the intervention-associated changes of each metric. Finally we weighted these maps of feature differences with the feature impact. This yielded spatial maps that condense the modulation, importance and informativeness of each metric at each location for a compact visual interpretation. We denote this combination as the *feature-weighted* impact. For a more specific analysis of these three aspects one can also visualize these maps individually, depending on the requirements of MRI study. An implementation including a demo version is available at: <https://github.com/simonvino/FuSL> which is based on functionalities provided by

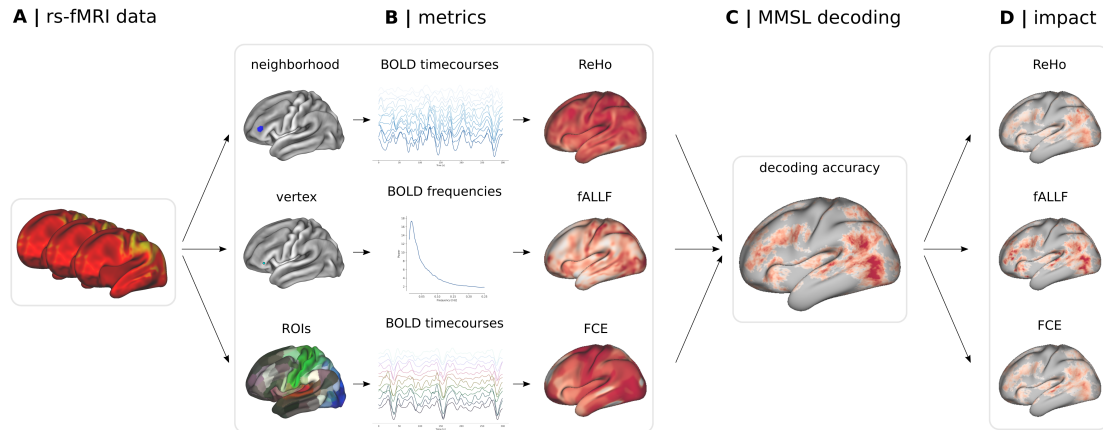


Figure 1: Individual steps of the FuSL framework. (A) In resting-state fMRI we can observe a BOLD signal exhibiting complex spatial and temporal dynamics. (B) Using different metrics we can characterize different aspects of these neural dynamics. Regional homogeneity (ReHo) quantifies the coherence of the BOLD signal within local neighborhoods across the cortex. Fractional amplitudes of low frequency fluctuations (fALLF) are defined as the ratio of the low-frequency power to the power of the entire frequency range for each vertex. Functional connectivity can be used to characterize functional connection efficiency (FCE) of individual ROIs in the global brain network. (C) In our FuSL framework these different metrics are concatenated to identify brain regions that are informative for decoding a brain state. (D) We used Shapley additive explanations (SHAP) to retrospectively reconstruct the impact of each metric on the decoding at a specific location.

NiLearn² (Abraham et al., 2014), scikit-learn³ (Pedregosa et al., 2011), and the SHAP software package⁴ (Lundberg and Lee, 2017).

2.2 Datasets

2.2.1 Artificial dataset

In the beginning we use an artificial dataset to investigate basic properties of FuSL when combining different data sources. On one side we want to study decoding performance of FuSL when signal or information is present in multiple imaging metrics or modalities simultaneously in the same location. On the other side we explore the behavior when we combine noisy non-informative data sources with informative ones in our FuSL. To study these scenarios we generate 3 artificial source signals, which could represent 3 different neuroimaging metrics or modalities. In this toy example the objective of the FuSL is, based on these 3 sources, to discriminate between two groups. We generated data for two groups, each containing 30 samples, by inducing artificial signals in one group, but not the other. Therefore we set signal values to 1 within a circular region of interest (ROI). In source 1 and 2 we simultaneously induce a signal in the left frontal cortex setting values within a 5 mm radius to 1 and -1 respectively (defined as ROI 1). As a third source we induced a signal in the left parietal cortex, setting values to 1 within a 5 mm radius (defined as ROI 2). We then generated multiple samples from these signals by sampling the signal amplitudes from a Gaussian normal distribution with standard deviation of 1, to simulate signal variability as observed in biological fMRI data. We additionally added random Gaussian noise to each sample with varying powers $P_{noise} = [0.1, 1, 2]$ resulting in three

²<https://nilearn.github.io/stable/index.html>

³<https://scikit-learn.org/stable/>

⁴<https://shap.readthedocs.io/en/latest/>

different datasets with signal to noise ratios $S/N = [2, 1, 0.1]$ respectively. In this manner we created datasets for which signals in source 1 and 2 overlapped in ROI 1, and one signal was only expressed in ROI 2 in source 3.

2.2.2 Resting-state fMRI dataset

Study description We used rs-fMRI data of 34 subjects who underwent rs-fMRI after a five days intake of either alprazolam or placebo (Wein et al., 2024). Participants gave their written informed consent at the beginning of the experiment and the study was approved by the local ethics committee (approval number 18-1197-111) and the National Institute for Pharmaceutical Security (BfArM, Eudra-CT-number: 2018-002181-40). Subjects received alprazolam (1.5 mg/d in 3 doses of 0.5 mg) or placebo for 5 days, each with at least 7 days washout phases between treatments.

MRI acquisition Resting-state fMRI data were collected with a Siemens Magnetom Prisma 3T Scanner at the University of Regensburg. Participants were instructed to relax and stay awake during the rs-fMRI session, while keeping their eyes closed. Based on pre-studies on optimizing the signal to noise ratio of echoplanar imaging (EPI) protocols (Seidel et al., 2020), we used an EPI multi-band sequence (multi-band factor 4) with a repetition time (TR) of 1000 ms, echo time (TE) of 30 ms and a flip angle (FA) of 60° . During a scanning time of 22 min in total 1320 volumes were collected, with a field of view (FoV) of $192 \text{ mm} \times 192 \text{ mm}$, an acquisition matrix (AM) of 64×64 , and an isotropic voxel size of 3 mm. Additionally field map images were collected by using a double-echo spoiled gradient echo sequence, with TR = 715 ms, TE = 5.81/8.27 ms, FA = 40° , with an isotropic voxel size of 3 mm, generating a magnitude image and two phase images. High resolution T1-weighted images were acquired using a Magnetization Prepared Rapid Gradient Echo (MP-RAGE) sequence, with a TR = 1919 ms, TE = 3.67 ms, FA = 9° , AM = 256×256 and FoV = $250 \text{ mm} \times 250 \text{ mm}$.

Preprocessing For preprocessing the functional and structural imaging data, we incorporated the processing pipeline provided by fMRIPrep⁵ (version 20.2.4) (Esteban et al., 2017) which included bias field correction, motion correction, slice timing correction and projection onto the cortical surface, generating high-resolution grayordinate time courses in the fsLR standard space (Glasser et al., 2013). Prior to the ReHo and fALFF analysis we smoothed the fMRI data using Gaussian surface smoothing with a FWHM of 3 mm (Glasser et al., 2013).

Resting-state fMRI metrics For computing regional homogeneity (ReHo), we selected for each vertex its 5-hop neighboring vertices in the fsLR standard space (Glasser et al., 2013), and computed ReHo as the average Pearson correlation between neighbouring BOLD time courses within the 0.01 Hz - 0.1 Hz frequency range. To analyze fractional amplitude of low frequency fluctuations (fALFF) we focused on the very-low frequency range 0.01 Hz - 0.05 Hz, which has been reported to increase during midazolam sedation and anesthesia (Kiviniemi et al., 2000, 2003, 2005). We computed fALFF as the ratio of the BOLD signal's power spectrum of these very low-frequencies to the signal's entire frequency range. To evaluate whole-brain FC we subdivided each hemisphere into 180 ROIs defined by Glasser et al. (2016). We computed the average activity time course within each ROI and filtered the resting-state BOLD signal within the 0.01 Hz - 0.1 Hz low frequency range. FC was then defined as the Pearson correlation coefficient r between time courses of pairs of ROIs to obtain a 360×360 whole-brain FC matrix. We selected a moderate FC threshold $r \geq 0.6$ yielding an average connection density of 39.2% and analyzed modulations in functional connectivity efficiency (FCE) for each ROI

⁵<https://fmriprep.org/en/stable/>

in the network. According to the weights of the probabilistic multi-modal parcellation (Glasser et al., 2016), for each vertex we computed FCE as a weighted sum of the ROI-wise FCE values, weighting each vertex with the probability to belong to a respective ROI. This yielded a spatially continuous distribution of FCE values across vertices. A mathematical definition of these three metrics is additionally provided in supplement I.

3 Results

3.1 Artificial dataset

We first investigated basic properties of the FuSL framework using the artificial dataset. Figure 2 (A) illustrates the 2 ROIs with artificial signals, whereby signal in ROI 1 is observed in sources 1 and 2, whereas the signal in ROI 2 is only observed in source 3, as depicted in figure 2 (B). We sampled signal amplitudes from a Gaussian normal distribution (with mean $\mu = 0$ and standard deviation $\sigma = 1$) and added noise with a power of $P_{noise} = 1$, resulting in an average signal to noise ratio of $S/N = 1$. An example of one sample with a noisy signal is shown in figure 2 (C). We then studied the decoding accuracy using different combinations of these sources as inputs for the FuSL. To fit the FuSL we used 10-fold stratified CV with 10 repetitions and used a SL radius of 3 vertices. As a decoder we employed a support vector classifier with a radial basis function kernel (Cortes and Vapnik, 1995; Schölkopf et al., 1998). Figure 2 (D) shows statistically significant decoding accuracy across the cortex when one incorporates all three sources simultaneously. In ROI 1 we observed higher decoding accuracy values than in ROI 2, because in ROI 1 the FuSL classifier could combine information simultaneously present in source 1 and 2. We then reconstructed the impact, as well as the feature-weighted impact of each source, as shown in figure 2 (E) and (F). Impact values of source 1 and 2 are higher in ROI 1 than in ROI 2, and of source 3 higher in ROI 2 than in ROI 1. Further we can see that feature-weighted impact maps reflected well the ground truth signals shown in figure 2 (B), whereby we observed some variability due to the added noise. Incorporating differences in features between groups in these maps also allowed us to reconstruct the change of the signal in each source. In this manner we were able to retrieve the increase of the signal in source 1 and decrease of the signal in source 2.

We then studied the decoding accuracy under different combinations of informative and uninformative data sources as inputs for FuSL. For the statistical testing of accuracy differences across CV folds, we employed a paired t-test incorporating variance correction proposed by Nadeau and Bengio (1999) to account for correlations in the training data across folds, and repeated 10-fold CV 10 times to obtain a reliable estimate (Bouckaert and Frank, 2004). We applied false discovery rate (FDR) correction to account for multiple comparisons of different combinations of sources (Benjamini and Hochberg, 1995). Figure 2 (G) shows the average decoding accuracies in ROI 1 for all combinations of the three modalities. We defined a combination of two sources using the $||$ operator, indicating a concatenation of their features. Using only source 1 or source 2 as input leads to an accuracy of 82.5% and 81.1% respectively, whereby using their combination $1||2$ in FuSL increases the accuracy to 90.6% (Cohen’s $d = 0.856$ and $d = 0.729$ respectively). Adding data source 3, which has no signal in ROI 1 slightly decreases the decoding accuracy to 90.2% in ROI 1 (Cohen’s $d = 0.043$). In ROI 2 an average accuracy of 81.9% is achieved when using only the informative source 3 as an input, as shown in figure 2 (H). The performance decreases slightly but significantly to 80.3% and 80.2% when noisy, uninformative sources are added (Cohen’s $d = 0.138$ and $d = 0.150$ respectively), and to 79.7% when two uninformative sources are added (Cohen’s $d = 0.200$). Figure 2 (I) shows the average decoding accuracy of ROI 1 and 2. We observed that a combination of all sources $1||2||3$ achieved the overall best decoding accuracy. The increase in decoding accuracy by adding an informative source is thereby considerably larger than the decrease when adding an uninformative

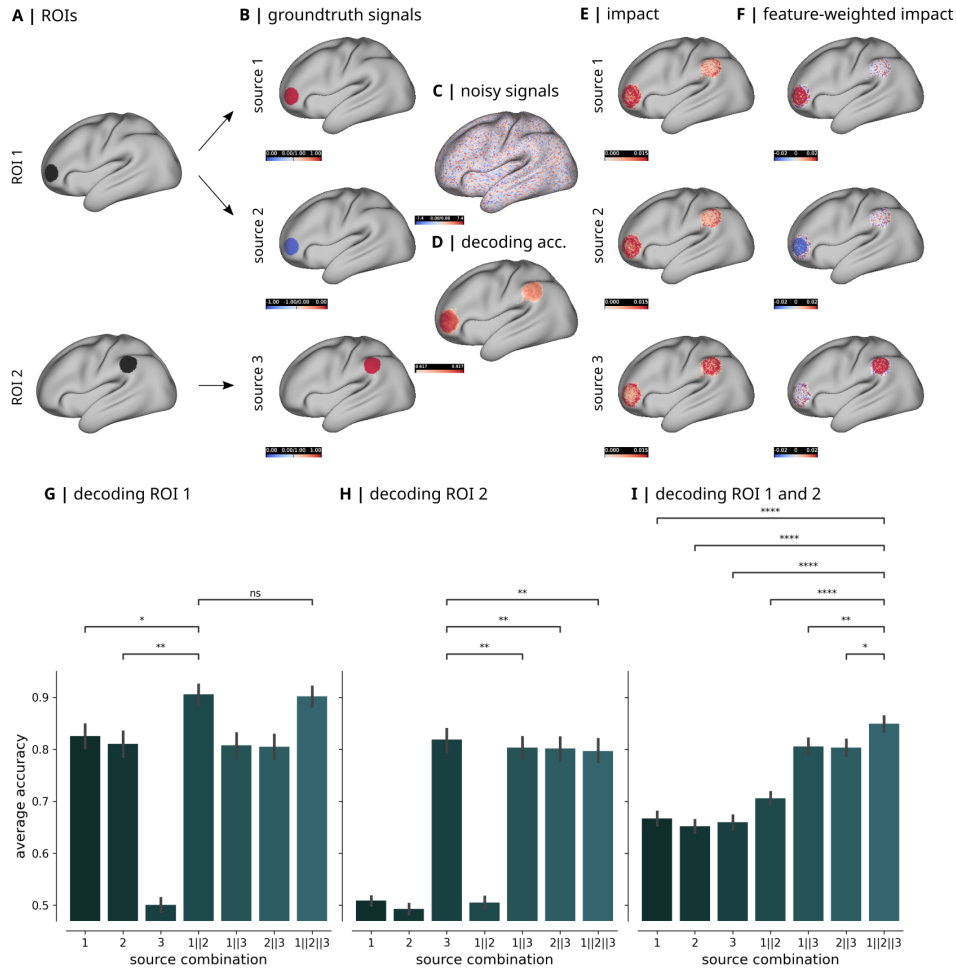


Figure 2: Investigating basic properties of the FuSL framework using an artificial dataset. We induce artificial signals in two ROIs (A), whereby signals of source 1 and 2 overlap in ROI 1 and signals in source 3 are only present in ROI 2 (B). (C) We then generate samples by randomly varying the signal amplitude and adding Gaussian noise. (D) We observe higher decoding accuracy values in ROI 1 than in ROI 2. (E) Impact values of source 1 and 2 are higher in ROI 1 than ROI 2, and of source 3 higher in ROI 2 than ROI 1. (F) The feature-weighted impact displays increased values in source 1 and 3 and the decrease of values in source 2. (G) and (H) show decoding accuracies for all combinations of sources in ROI 1 and 2 respectively. (I) Decoding accuracies averaged across ROI 1 and 2. Error bars represent 95% confidence intervals across folds. Significant differences of accuracies in figure (G), (H) and (I) are indicated with: *: $p \leq 0.05$, **: $p \leq 0.01$, ***: $p \leq 0.001$, ****: $p \leq 0.0001$, ns: not significant, (ns): not significant after false discovery rate correction.

source, even in this scenario of relatively high noise levels ($S/N = 1$). We observed a similar behavior when combining sources with higher ($S/N = 2$) and lower ($S/N = 0.1$) signal to noise ratio in supplement II figure S1.

We further demonstrate in an example, how reconstructing feature importance using Shapley values increased also the spatial specificity of detected regions that were relevant for decoding a brain state. To this aim, we generated a signal in one vertex on the surface as shown in figure 3 (A). Current applications typically report the entire area of SLs with significant decoding accuracy (Etzel et al., 2013; Viswanathan et al., 2012), which is shown in our example in figure 3 (B). This area can be considerably larger than the area of the actual signal, because all SLs that contain the informative vertex may be able to successfully decode. Computing feature importance on vertex-level based on Shapley values allowed us to trace back the exact location of an important vertex within a SL. If we then average importance values across overlapping SLs, and weight these maps with the decoding accuracy, the map of feature impact can precisely identify the original location of the signal, as shown in figure 3 (C).

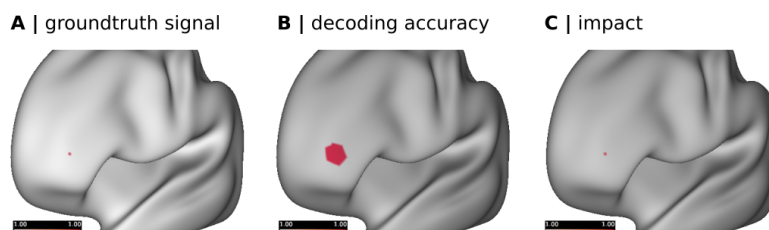


Figure 3: Increasing spatial specificity of searchlight decoding using Shapley values. (A) We induce a signal in one vertex only. (B) The area of significant decoding accuracy is considerably larger than the original signal. (C) Analyzing the feature impact maps allows us to reconstruct again the exact location of an informative vertex.

3.2 Resting-state fMRI dataset

Here, we study how integrating complementary rs-fMRI metrics in FuSL can improve the prediction of pharmacological treatment in rs-fMRI data. We incorporated combinations of regional homogeneity (ReHo), fractional amplitude of low frequency fluctuations (fALFF) and functional connectivity efficiency (FCE) with the objective to predict whether participants have received the sedative alprazolam or a placebo. We split the data of 34 subjects into train and test data using stratified 10-fold CV. For statistical comparison of model accuracies we repeated 10-fold CV 100 times and used a paired t-test including variance correction (Nadeau and Bengio, 1999) and FDR correction (Benjamini and Hochberg, 1995). Figure 4 (A) shows the performance of FuSL related to different combinations of rs-fMRI metrics. Decoding accuracies averaged across the cortex are depicted in figure 4 (A1). Respective p-values and effect sizes are provided in supplement table S1. We further evaluated the number of vertices where FuSL was able to find significant differences between groups, using 10-fold CV and TFCE permutation-based correction with 1000 permutations. Average TFCE weighted accuracy values and the proportion of significant vertices are shown in figure 4 (A2) and (A3) respectively. The combinations ReHo||FCE and ReHo||fALFF||FCE achieved the highest average decoding accuracies, whereby threshold-free cluster enhanced accuracies and the number of significant (TFCE corrected) vertices were highest for the combination ReHo||fALFF||FCE.

To illustrate which significant vertices could be additionally detected when combining all three rs-fMRI metrics, figure 4 (B) shows the differences between ReHo||fALFF||FCE and all other possible combinations of metrics. When using ReHo, FCE or ReHo||FCE, no area on the

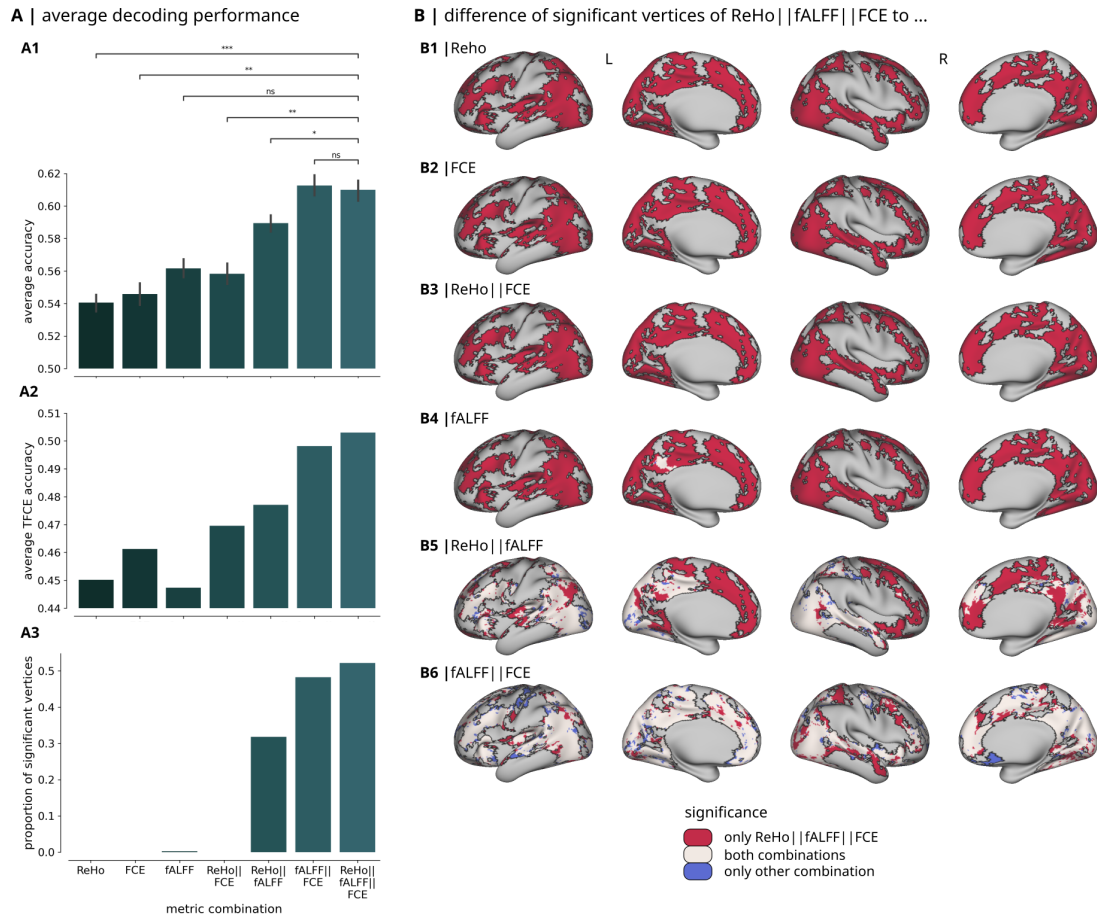


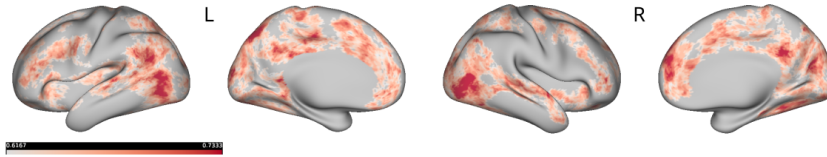
Figure 4: Decoding performance of FuSL in dependency of metric combinations. (A) Decoding performance averaged across the whole cortex. (A1) Combinations of fALFF||FCE and ReHo||fALFF||FCE achieved the highest average decoding accuracies. (A2) The combination ReHo||fALFF||FCE yielded highest threshold-free cluster enhanced accuracy values. (A3) The combination ReHo||fALFF||FCE also produced the highest number of significant vertices. (B) Areas that can be additionally decoded when using the combination ReHo||fALFF||FCE in FuSL. Locations where only ReHo||fALFF||FCE yielded significant decoding accuracies are highlighted in red in the left (L) and right (R) cortex. Locations where ReHo||fALFF||FCE and the respective other combination can both significantly decode are marked in white. Locations where only the respective other combination is able to decode are depicted in blue. Significant differences of accuracies in figure (A) are indicated with: *: $p \leq 0.05$, **: $p \leq 0.01$, ***: $p \leq 0.001$, ns: not significant.

cortex showed significant decoding accuracy. By using a combination of all three rs-fMRI metrics (ReHo||fALFF||FCE) we could find significant alterations in various typical resting-state networks (Yeo et al., 2011), as highlighted in red in figures 4 (B1), (B2) and (B3). Due to the administration of alprazolam we found modulations in large parts of the visual resting-state network across the full occipital cortex. In the default mode network we observe effects in the parietal cortex, inferior frontal gyrus, superior temporal gyrus, and the anterior and posterior cingulate cortex. In the dorsal attention resting-state network we found differences within the inferior temporal cortex, superior parietal lobule, angular gyrus and left precentral gyrus. Further we observe modulations predominantly in the frontal parts of the frontoparietal network, and modulations of the ventral attention network mainly in the anterior and posterior cingulate gyrus. In the somatomotor resting-state network we found an effect in the precentral gyrus. A detailed overlay of regions with these significant decoding accuracies and the resting-state atlas defined by Yeo et al. (2011) is provided in supplement II figure S2. Figure 4 (B4) shows the comparison to the case when using only fALFF as input. Both variants could detect significant alterations within the default mode network in the posterior cingulate cortex (overlap highlighted in white), but only using fALFF did not allow us to decode in any other region. Further the difference to the combination of ReHo||fALFF is illustrated in figure 4 (B5). A combination of ReHo||fALFF enabled us to also successfully decode within the visual, frontoparietal, ventral/dorsal attention and default resting-state network, but failed to decode in the motor cortex and large parts of the default network within the cingulate cortex and superior frontal gyrus. A small number of vertices that became significant incorporating a combination of ReHo||fALFF but not ReHo||fALFF||FCE are marked in blue. Finally differences between fALFF||FCE and ReHo||fALFF||FCE are depicted in figure 4 (B6). Here we can observe that on the one side a combination fALFF||FCE was able to additionally decode some more vertices within the left and right somatosensory network and left limbic network. On the other side a combination of ReHo||fALFF||FCE allowed to capture more vertices within the default network in the superior temporal sulcus, right frontoparietal and dorsal attention network. Overall a combination of all three rs-fMRI metrics (ReHo||fALFF||FCE) yielded the highest number of vertices with statistically significant decoding accuracies.

We then studied in detail the impact of each metric in the FuSL that combines all three rs-fMRI metrics (ReHo||fALFF||FCE). Figure 5 (A) shows statistically significant decoding accuracies across the cortex. Within these regions we can observe highest discrimination capabilities in the visual network within the extrastriate cortex and in the default mode network within left angular gyrus, right anterior cingulate cortex and bilateral in posterior cingulate cortex. Analyzing the impact and feature-weighted impact of individual rs-fMRI metrics allowed us to relate the decoding performance to the individual input metrics. A comparison between the impact and feature-weighted impact shows that the magnitudes of these measures coincide qualitatively very well (supplementary figure S3), but analyzing the feature-weighted impact additionally allows one to identify, whether a metric is increase or decreased due to the alprazolam treatment. In figure 5 (B1) we could observe that for ReHo a decrease within the visual network in the right extrastriate cortex is most indicative for the administration of alprazolam. Further we observed a characteristic decrease of ReHo mainly in frontal parts of the frontoparietal resting-state network, and within the default mode network a decrease in the parietal and posterior cingulate cortex. Simultaneously we found an increase in ReHo in the somatomotor network, and within the default mode network an increase in the anterior cingulate cortex. In comparison to ReHo, for fALFF we observed generally higher feature-weighted impact values across the cortex, as illustrated in figure 5 (B2). A characteristic increase of fALFF due to alprazolam can be found within the visual network bilateral in the extrastriate cortex. Additionally we found an increase with high impact in fALFF within the frontoparietal and default mode network, in frontal cortex, and anterior and posterior cingulate cortex. Related to alprazolam we found predominantly a decrease of FCE as shown in figure 5 (B3). This decrease of FCE has highest impact on the

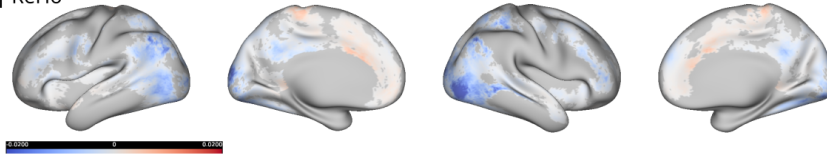
decoding also within the visual network in the extrastriate cortex, and within the default mode network in the superior temporal gyrus. Additionally an overlay of the decoding accuracy map and feature-weighted impact maps with the resting-state network atlas established by [Yeo et al. \(2011\)](#) is provided in supplement II figure S4.

A | decoding accuracy

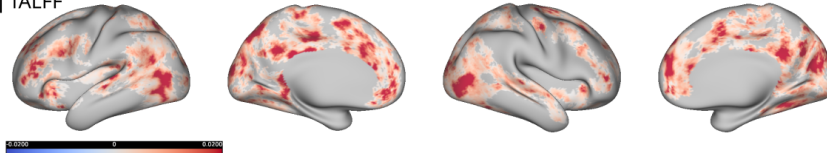


B | feature-weighted impact

B1 | ReHo



B2 | fALFF



B3 | FCE

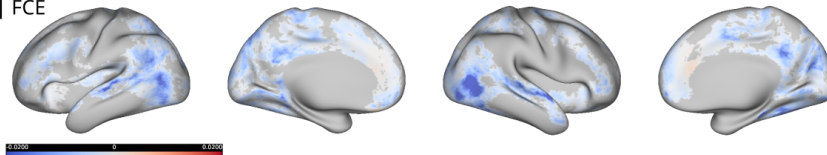


Figure 5: (A) Combining ReHo, fALFF and FCE in FuSL yields highest decoding accuracies in the visual network and frontal part of the default mode network. (B) The feature-weighted impact illustrates the informativeness, importance and relative increase or decrease of these metric, related to the treatment of alprazolam. (B1) Illustrates the decrease of ReHo mainly in the visual and frontoparietal network, including frontal parts of the default mode network. Simultaneously we observe an increase in ReHo in the somatomotor network and anterior cingulate cortex. (B2) A characteristic increase in fALFF can be found mainly in the visual, frontoparietal and default mode network. (B3) A high feature-weighted impact related to a decrease of FCE is highest within the visual network in the extrastriate cortex and default mode network in the superior temporal gyrus.

4 Discussion

In our study we presented an interpretable SL framework for fusing the complementary information of different rs-fMRI metrics. We first used an artificial dataset to study how different combinations of informative and uninformative data sources can affect decoding capabilities of FuSL. We demonstrated that across different signal to noise ratios the gain of adding informative sources exceeded the loss in performance when adding an uninformative source (2). We further illustrated how reconstructing feature-importance using SHAP can recover the impact of each data source, as well as the exact location of informative vertices. In a next step we studied how combining ReHo, fALFF and FCE can enhance the prediction of pharmacological treat-

ment in rs-fMRI. Decoding based on combinations of different rs-fMRI metrics outperformed consistently decoding based on single metrics (figure 4). A combination of measuring localized fluctuations in low-frequency fluctuations and global connectivity efficiency (fALFF||FCE), as well as the combination of all three metrics (ReHo||fALFF||FCE), achieved highest decoding performances. Especially in clinical studies where collecting a very large sample size is often not feasible, the integration of different information sources can help improving decoding sensitivity on smaller datasets. Still, how distinct rs-fMRI markers are coupled and related to each other is not yet investigated and understood in detail (Lv et al., 2018). Our comparisons show that metrics derived from the same signal can exhibit very distinct characteristics in different areas across the cortex. For instance in the somatomotor network we observed an increase both in fALFF and ReHo, but within the visual network we observed an increase in fALFF whereas ReHo decreased. Note that the interrelations of rs-fMRI markers and their optimal combination in FuSL might therefore also vary between different rs-fMRI studies. It has yet to be shown which of the patterns reported here will remain stable across different studies. Furthermore, we have shown how one can utilize explainable AI to reconstruct the impact of each rs-fMRI metric on the decoding in our workflow. Incorporating the SHAP framework (Lundberg and Lee, 2017) allowed us to analyze locally the importance of features (in our study rs-fMRI metrics), which we combined with local informativeness (derived from decoding accuracy) to quantify the impact of a feature across the cortex. We propose to additionally incorporate local differences in features between groups to visualize whether a feature-expression increases or decreases. In theory a large feature difference does not necessarily correlate with a high feature impact, because the output of a non-linear decoding model can depend on a highly non-linear combination of its input features. In our practical application we however observed that absolute amplitudes of the impact and feature-weighted impact corresponded qualitatively very well (supplementary figure S3), so for a compact interpretation we considered it useful to visualize the feature-weighted impact. Yet, to study the impact of a feature in more detail, we propose to additionally visualize the impact in isolation. Besides using SHAP for computing the differential impact of each metric, we have shown that incorporating explainable AI can be generally beneficial for searchlight analysis. Evaluating feature-importance of the decoding model could help to reconstruct the exact location of informative vertices or voxels, which makes this technique interesting for all types of searchlight decoding analysis.

Studying the feature-weighted impact of individual rs-fMRI markers could reveal different effects of the alprazolam treatment on brain functions. For example, the sedation-typical increase in fALFF (Kiviniemi et al., 2003, 2005) and decrease in FCE (Wei et al., 2013; Hashmi et al., 2017; Schrouff et al., 2011) in low-level sensory regions could relate to several well-studied behavioral side effects of alprazolam. Observed modulations in the motor and visual cortices might be connected to motor coordination impairments and visuospatial and visuomotor abilities related to benzodiazepines (Griffin et al., 2013; Golombok et al., 1988; Tata et al., 1994). The decrease in ReHo and FCE in more high-level areas might be connected to impairments in cognitive domains such as attention, working memory and semantic processing, which are affected by long-term treatments with benzodiazepines (Barker et al., 2004; Stewart, 2005).

In our study we showed how fusing different metrics can improve SL decoding specifically in resting-state fMRI analysis. Our framework thereby leverages the strengths of SL decoding, inherently limiting model complexity by using spatially localized features, making it a robust tool for neuroimaging studies with smaller sample sizes. Furthermore using a model-agnostic approach for measuring feature importance based on Shapley values (Lundberg and Lee, 2017), our workflow allows one to integrate any kind of decoding model. Besides this application of decoding in rs-fMRI, our FuSL workflow can be easily adapted to various additional domains of neuroimaging. Combining different imaging modalities in FuSL could be beneficial for studying processes and conditions that simultaneously affect brain structure and function like observed in learning (Carreiras et al., 2009) or schizophrenia (Dabiri et al., 2022). Also this framework

would allow one to integrate activation maps of combined fMRI and EGG studies (Menon and Crottaz-Herbette, 2005). In this manner FuSL provides a flexible and interpretable tool for diverse applications in neuroimaging analysis.

Data and Code Availability

The codes including the artificial dataset are publicly available at: <https://github.com/simonvino/FuSL>. The resting-state fMRI dataset is available from the corresponding author on reasonable request.

Author Contributions

SW and JS designed the analysis. SW implemented the analysis. RR and CN were responsible for the clinical MRI study. MR, LMB and JS acquired the imaging data. SW, and JS wrote the initial draft. All authors revised the manuscript.

Funding

This work has been supported by the German Research Foundation (Deutsche Forschungsgemeinschaft) (DFG), project number 403161218, to JS and within the framework of FOR2858.

Declaration of Competing Interests

The authors declare no conflicts of interest.

References

- A. Abraham, F. Pedregosa, M. Eickenberg, P. Gervais, A. Mueller, J. Kossaifi, A. Gramfort, B. Thirion, and G. Varoquaux. Machine learning for neuroimaging with scikit-learn. *Frontiers in Neuroinformatics*, 8, 2014. ISSN 1662-5196. doi: 10.3389/fninf.2014.00014. URL <https://www.frontiersin.org/journals/neuroinformatics/articles/10.3389/fninf.2014.00014>.
- M. F. Ahamed, M. M. Hossain, M. Nahiduzzaman, M. R. Islam, M. R. Islam, M. Ahsan, and J. Haider. A review on brain tumor segmentation based on deep learning methods with federated learning techniques. *Computerized Medical Imaging and Graphics*, 110:102313, 2023. ISSN 0895-6111. doi: <https://doi.org/10.1016/j.compmedimag.2023.102313>. URL <https://www.sciencedirect.com/science/article/pii/S0895611123001313>.
- M. Barker, K. Greenwood, M. Jackson, and S. Crowe. Cognitive effects of long-term benzodiazepine use - a meta-analysis. *Cns Drugs*, 18:37–48, 01 2004.
- D. Bassett and O. Sporns. Network neuroscience. *Nature Neuroscience*, 20:353–364, 02 2017. doi: 10.1038/nn.4502.
- Y. Benjamini and Y. Hochberg. Controlling the false discovery rate: A practical and powerful approach to multiple testing. *Journal of the Royal Statistical Society. Series B (Methodological)*, 57(1):289–300, 1995. ISSN 00359246. URL <http://www.jstor.org/stable/2346101>.
- B. B. Biswal, F. Z. Yetkin, V. Haughton, and J. S. Hyde. Functional connectivity in the motor cortex of resting human brain using echo-planar mri. *Magnetic Resonance in Medicine*, 34, 1995.
- L. Blanco-Hinojo, J. Pujol, D. Macià, G. Martínez-Vilavella, R. Martín-Santos, P. Victor, and J. Deus. Mapping the synchronization effect of gamma-aminobutyric acid inhibition on the cerebral cortex using magnetic resonance imaging. *Brain Connectivity*, 11, 04 2021. doi: 10.1089/brain.2020.0844.
- R. Bouckaert and E. Frank. Evaluating the replicability of significance tests for comparing learning algorithms. volume 3056, pages 3–12, 01 2004. doi: 10.1007/978-3-540-24775-3_3.
- J. Cabral, M. L. Kringelbach, and G. Deco. Exploring the network dynamics underlying brain activity during rest. *Progress in Neurobiology*, 114:102–131, 2014. ISSN 0301-0082. doi: <https://doi.org/10.1016/j.pneurobio.2013.12.005>. URL <https://www.sciencedirect.com/science/article/pii/S0301008213001457>.
- V. D. Calhoun and J. Sui. Multimodal fusion of brain imaging data: A key to finding the missing link(s) in complex mental illness. *Biological Psychiatry: Cognitive Neuroscience and Neuroimaging*, 1(3):230–244, 2016. ISSN 2451-9022. doi: <https://doi.org/10.1016/j.bpsc.2015.12.005>. URL <https://www.sciencedirect.com/science/article/pii/S2451902216000598>. Brain Connectivity in Psychopathology.
- M. Carreiras, M. Seghier, S. Baquero Castellanos, A. Estévez, A. Lozano-Castillo, J. Devlin, and C. Price. An anatomical signature for literacy. *Nature*, 461:983–6, 10 2009. doi: 10.1038/nature08461.
- R. M. Cichy and A. Oliva. A m/eeg-fmri fusion primer: Resolving human brain responses in space and time. *Neuron*, 107(5):772–781, 2020. ISSN 0896-6273. doi: <https://doi.org/10.1016/j.neuron.2020.07.001>. URL <https://www.sciencedirect.com/science/article/pii/S0896627320305183>.

- R. M. Cichy, D. Pantazis, and A. Oliva. Similarity-Based Fusion of MEG and fMRI Reveals Spatio-Temporal Recognition. *Cerebral Cortex*, 26(8):3563–3579, 07 2016. ISSN 1047-3211. doi: 10.1093/cercor/bhw135. URL <https://doi.org/10.1093/cercor/bhw135>.
- C. Cortes and V. Vapnik. Support-vector networks. *Machine learning*, 20(3):273–297, 1995.
- M. Dabiri, F. Dehghani Firouzabadi, K. Yang, P. B. Barker, R. R. Lee, and D. M. Yousem. Neuroimaging in schizophrenia: A review article. *Frontiers in Neuroscience*, 16, 2022. ISSN 1662-453X. doi: 10.3389/fnins.2022.1042814. URL <https://www.frontiersin.org/journals/neuroscience/articles/10.3389/fnins.2022.1042814>.
- O. Esteban, R. Blair, C. J. Markiewicz, S. L. Berleant, C. Moodie, F. Ma, A. I. Isik, A. Erramuzpe, M. Goncalves, R. A. Poldrack, and K. J. Gorgolewski. poldracklab/fmriprep: 1.0.0-rc5, Sept. 2017. URL <https://doi.org/10.5281/zenodo.996169>.
- J. A. Etzel, J. M. Zacks, and T. S. Braver. Searchlight analysis: Promise, pitfalls, and potential. *NeuroImage*, 78:261–269, 2013. ISSN 1053-8119. doi: <https://doi.org/10.1016/j.neuroimage.2013.03.041>. URL <https://www.sciencedirect.com/science/article/pii/S1053811913002917>.
- Y. Gao, X. Wang, Z. Xiong, H. Ren, R. Liu, Y. Wei, and D. Li. Abnormal fractional amplitude of low-frequency fluctuation as a potential imaging biomarker for first-episode major depressive disorder: A resting-state fmri study and support vector machine analysis. *Frontiers in Neurology*, 12, 2021. ISSN 1664-2295. doi: 10.3389/fneur.2021.751400. URL <https://www.frontiersin.org/journals/neurology/articles/10.3389/fneur.2021.751400>.
- M. Glasser, S. Sotiropoulos, J. Wilson, T. Coalson, B. Fischl, J. Andersson, J. Xu, S. Jbabdi, M. Webster, J. Polimeni, V. DC, and M. Jenkinson. The minimal preprocessing pipelines for the human connectome project. *NeuroImage*, 80:105, 10 2013. doi: 10.1016/j.neuroimage.2013.04.127.
- M. Glasser, T. Coalson, E. Robinson, C. Hacker, J. Harwell, E. Yacoub, K. Ugurbil, J. Andersson, C. Beckmann, M. Jenkinson, S. Smith, and D. Van Essen. A multi-modal parcellation of human cerebral cortex. *Nature*, 536, 07 2016. doi: 10.1038/nature18933.
- S. Golombok, P. Moodley, and M. Lader. Cognitive impairment in long-term benzodiazepine users. *Psychological Medicine*, 18(2):365–374, 1988.
- A. S. Greene, C. Horien, D. Barson, D. Scheinost, and R. T. Constable. Why is everyone talking about brain state? *Trends in Neurosciences*, 46(7):508–524, 2023. ISSN 0166-2236. doi: <https://doi.org/10.1016/j.tins.2023.04.001>. URL <https://www.sciencedirect.com/science/article/pii/S0166223623001017>.
- C. E. Griffin, A. M. Kaye, F. R. Bueno, and A. D. Kaye. Benzodiazepine pharmacology and central nervous system-mediated effects. *The Ochsner journal*, 13 2:214–23, 2013.
- J. A. Hashmi, M. L. Loggia, S. Khan, L. Gao, J. Kim, V. Napadow, E. N. Brown, and O. Akeju. Dexmedetomidine Disrupts the Local and Global Efficiencies of Large-scale Brain Networks. *Anesthesiology*, 126(3):419–430, 03 2017. ISSN 0003-3022. doi: 10.1097/ALN.0000000000001509.
- J. Huang, M. Li, Q. Li, Z. Yang, B. Xin, Z. Qi, Z. Liu, H. Dong, K. Li, Z. Ding, and J. Lu. Altered functional connectivity in white and gray matter in patients with multiple sclerosis. *Frontiers in Human Neuroscience*, 14, 2020. ISSN 1662-5161. doi:

- 10.3389/fnhum.2020.563048. URL <https://www.frontiersin.org/journals/human-neuroscience/articles/10.3389/fnhum.2020.563048>.
- N. Javaheripour, M. li, T. Chand, A. Krug, T. Kircher, U. Dannlowski, I. Nenadić, J. P. Hamilton, M. Sacchet, I. Gotlib, H. Walter, T. Frodl, S. Grimm, B. Harrison, C. Wolf, S. Olbrich, G. van Wingen, L. Pezawas, G. Parker, and G. Wagner. Altered resting-state functional connectome in major depressive disorder: a mega-analysis from the psymri consortium. *Translational Psychiatry*, 11:511, 10 2021. doi: 10.1038/s41398-021-01619-w.
- L. Jiang and X.-N. Zuo. Regional homogeneity: A multimodal, multiscale neuroimaging marker of the human connectome. *The Neuroscientist*, 22(5):486–505, 2016. doi: 10.1177/1073858415595004. URL <https://doi.org/10.1177/1073858415595004>. PMID: 26170004.
- R. H. Kaiser, J. R. Andrews-Hanna, T. D. Wager, and D. A. Pizzagalli. Large-Scale Network Dysfunction in Major Depressive Disorder: A Meta-analysis of Resting-State Functional Connectivity. *JAMA Psychiatry*, 72(6):603–611, 06 2015. ISSN 2168-622X. doi: 10.1001/jamapsychiatry.2015.0071. URL <https://doi.org/10.1001/jamapsychiatry.2015.0071>.
- V. Kiviniemi, J. Jauhiainen, O. Tervonen, E. Pääkkö, J. Oikarinen, V. Vainionpää, H. Rantala, and B. Biswal. Slow vasomotor fluctuation in fMRI of anesthetized child brain. *Magnetic Resonance in Medicine*, 44(3):373–378, 2000. doi: [https://doi.org/10.1002/1522-2594\(200009\)44:3<373::AID-MRM5>3.0.CO;2-P](https://doi.org/10.1002/1522-2594(200009)44:3<373::AID-MRM5>3.0.CO;2-P).
- V. Kiviniemi, J.-H. Kantola, J. Jauhiainen, A. Hyvärinen, and O. Tervonen. Independent component analysis of nondeterministic fMRI signal sources. *NeuroImage*, 19(2):253–260, 2003. ISSN 1053-8119. doi: [https://doi.org/10.1016/S1053-8119\(03\)00097-1](https://doi.org/10.1016/S1053-8119(03)00097-1).
- V. Kiviniemi, H. Haanpää, J.-H. Kantola, J. Jauhiainen, V. Vainionpää, S. Alahuhta, and O. Tervonen. Midazolam sedation increases fluctuation and synchrony of the resting brain bold signal. *Magnetic resonance imaging*, 23:531–7, 06 2005. doi: 10.1016/j.mri.2005.02.009.
- R. Kohavi. A study of cross-validation and bootstrap for accuracy estimation and model selection. In *Proceedings of the 14th International Joint Conference on Artificial Intelligence - Volume 2, IJCAI’95*, page 1137–1143, San Francisco, CA, USA, 1995. Morgan Kaufmann Publishers Inc. ISBN 1558603638.
- N. Kriegeskorte, R. Goebel, and P. Bandettini. Information-based functional brain mapping. *Proceedings of the National Academy of Sciences*, 103(10):3863–3868, 2006. doi: 10.1073/pnas.0600244103. URL <https://www.pnas.org/doi/abs/10.1073/pnas.0600244103>.
- Y. Liu, B. Meng, C. Zeng, J. Wang, Y. Li, P. Yin, S. K. Sah, and Y. Li. Abnormal baseline brain activity in patients with multiple sclerosis with simple spinal cord involvement detected by resting-state functional magnetic resonance imaging. *Journal of Computer Assisted Tomography*, 39(6):866–875, 2015.
- S. M. Lundberg and S.-I. Lee. A unified approach to interpreting model predictions. In *Proceedings of the 31st International Conference on Neural Information Processing Systems, NIPS’17*, page 4768–4777, Red Hook, NY, USA, 2017. Curran Associates Inc. ISBN 9781510860964.
- H. Lv, Z. Wang, E. Tong, L. Williams, G. Zaharchuk, M. Zeineh, A. Goldstein-Piekarski, T. Ball, C. Liao, and M. Wintermark. Resting-state functional mri: Everything that nonexperts have

- always wanted to know. *American Journal of Neuroradiology*, 2018. ISSN 0195-6108. doi: 10.3174/ajnr.A5527. URL <https://www.ajnr.org/content/early/2018/01/18/ajnr.A5527>.
- V. Menon and S. Crottaz-Herbette. Combined eeg and fmri studies of human brain function. In *Neuroimaging, Part A*, volume 66 of *International Review of Neurobiology*, pages 291–321. Academic Press, 2005. doi: [https://doi.org/10.1016/S0074-7742\(05\)66010-2](https://doi.org/10.1016/S0074-7742(05)66010-2). URL <https://www.sciencedirect.com/science/article/pii/S0074774205660102>.
- C. Nadeau and Y. Bengio. Inference for the generalization error. In S. Solla, T. Leen, and K. Müller, editors, *Advances in Neural Information Processing Systems*, volume 12. MIT Press, 1999. URL https://proceedings.neurips.cc/paper_files/paper/1999/file/7d12b66d3df6af8d429c1a357d8b9e1a-Paper.pdf.
- S. Ni, S. Gao, C. Ling, J. Jiang, F. Wu, T. Peng, J. Sun, N. Zhang, and X. Xu. Altered brain regional homogeneity is associated with cognitive dysfunction in first-episode drug-naive major depressive disorder: A resting-state fmri study. *Journal of Affective Disorders*, 343:102–108, 2023. ISSN 0165-0327. doi: <https://doi.org/10.1016/j.jad.2023.10.003>. URL <https://www.sciencedirect.com/science/article/pii/S0165032723011837>.
- F. Pedregosa, G. Varoquaux, A. Gramfort, V. Michel, B. Thirion, O. Grisel, M. Blondel, P. Prettenhofer, R. Weiss, V. Dubourg, J. Vanderplas, A. Passos, D. Cournapeau, M. Brucher, M. Perrot, and E. Duchesnay. Scikit-learn: Machine learning in Python. *Journal of Machine Learning Research*, 12:2825–2830, 2011.
- J. Schrouff, V. Perlberg, M. Boly, G. Marrelec, P. Boveroux, A. Vanhaudenhuyse, M.-A. Bruno, S. Laureys, C. Phillips, M. Péligrini-Issac, P. Maquet, and H. Benali. Brain functional integration decreases during propofol-induced loss of consciousness. *NeuroImage*, 57(1):198–205, 2011. ISSN 1053-8119. doi: <https://doi.org/10.1016/j.neuroimage.2011.04.020>.
- M.-A. Schulz, B. Yeo, J. Vogelstein, J. Mourao-Miranada, J. Kather, K. Kording, B. Richards, and D. Bzdok. Different scaling of linear models and deep learning in ukbiobank brain images versus machine-learning datasets. *Nature Communications*, 11:4238, 08 2020. doi: 10.1038/s41467-020-18037-z.
- B. Schölkopf, C. Burges, and A. Smola. *Advances in kernel methods - support vector learning*. MIT Press, 12 1998.
- P. Seidel, S. M. Levine, M. Tahedl, and J. V. Schwarzbach. Temporal signal-to-noise changes in combined multislice-and in-plane-accelerated echo-planar imaging with a 20-and 64-channel coil. *Scientific Reports*, 10(1):1–9, 2020.
- L. S. Shapley. *17. A Value for n-Person Games*, pages 307–318. Princeton University Press, Princeton, 1953. ISBN 9781400881970. doi: [doi:10.1515/9781400881970-018](https://doi.org/10.1515/9781400881970-018). URL <https://doi.org/10.1515/9781400881970-018>.
- Z. Shen, L. Jiang, S. Yang, J. Ye, N. Dai, X. Liu, N. Li, J. Lu, F. Liu, Y. Lu, X. Sun, Y. Cheng, and X. Xu. Identify changes of brain regional homogeneity in early and later adult onset patients with first-episode depression using resting-state fmri. *PLOS ONE*, 12:1–16, 09 2017. doi: 10.1371/journal.pone.0184712. URL <https://doi.org/10.1371/journal.pone.0184712>.
- S. M. Smith and T. E. Nichols. Threshold-free cluster enhancement: Addressing problems of smoothing, threshold dependence and localisation in cluster inference. *NeuroImage*, 44(1):83–98, 2009. ISSN 1053-8119. doi: <https://doi.org/10.1016/j.neuroimage.2008>.

- 03.061. URL <https://www.sciencedirect.com/science/article/pii/S1053811908002978>.
- O. Sporns. *Networks of the Brain*. MIT Press, Cambridge, MA, 2010.
- S. Stewart. The effect of benzodiazepines on cognition. *The Journal of clinical psychiatry*, 66 Suppl 2:9–13, 02 2005.
- J.-f. Sun, L.-m. Chen, J.-k. He, Z. Wang, C.-l. Guo, Y. Ma, Y. Luo, D.-q. Gao, Y. Hong, J.-l. Fang, and F.-q. Xu. A comparative study of regional homogeneity of resting-state fmri between the early-onset and late-onset recurrent depression in adults. *Frontiers in Psychology*, 13, 2022. ISSN 1664-1078. doi: 10.3389/fpsyg.2022.849847. URL <https://www.frontiersin.org/journals/psychology/articles/10.3389/fpsyg.2022.849847>.
- L. E. Suárez, R. D. Markello, R. F. Betzel, and B. Misić. Linking structure and function in macroscale brain networks. *Trends in Cognitive Sciences*, 24(4):302–315, 2020. ISSN 1364-6613. doi: <https://doi.org/10.1016/j.tics.2020.01.008>. URL <https://www.sciencedirect.com/science/article/pii/S1364661320300267>.
- M. Tahedl, S. M. Levine, M. W. Greenlee, R. Weissert, and J. V. Schwarzbach. Functional connectivity in multiple sclerosis: Recent findings and future directions. *Frontiers in Neurology*, 9, 2018. ISSN 1664-2295. doi: 10.3389/fneur.2018.00828. URL <https://www.frontiersin.org/journals/neurology/articles/10.3389/fneur.2018.00828>.
- M. Tahedl, S. Levine, R. Weissert, Z. Kohl, D.-H. Lee, R. Linker, and J. Schwarzbach. Early remission in multiple sclerosis is linked to altered coherence of the cerebellar network. *Journal of Translational Medicine*, 20, 10 2022. doi: 10.1186/s12967-022-03576-4.
- P. R. Tata, J. Rollings, M. Collins, A. Pickering, and R. Jacobson. Lack of cognitive recovery following withdrawal from long-term benzodiazepine use. *Psychological Medicine*, 24(1): 203–213, 1994.
- M. P. van den Heuvel and H. E. Hulshoff Pol. Exploring the brain network: A review on resting-state fMRI functional connectivity. *European Neuropsychopharmacology*, 20 (8):519–534, 2010. ISSN 0924-977X. doi: <https://doi.org/10.1016/j.euroneuro.2010.03.008>. URL <https://www.sciencedirect.com/science/article/pii/S0924977X10000684>.
- S. Viswanathan, M. Cieslak, and S. T. Grafton. On the geometric structure of fmri searchlight-based information maps, 2012. URL <https://arxiv.org/abs/1210.6317>.
- X.-Y. Wang, H. Tan, X. Li, L.-Q. Dai, Z.-W. Zhang, F.-J. Lv, and R.-Q. Yu. Resting-state functional magnetic resonance imaging-based identification of altered brain the fractional amplitude of low frequency fluctuation in adolescent major depressive disorder patients undergoing electroconvulsive therapy. *Frontiers in Psychiatry*, 13, 2022. ISSN 1664-0640. doi: 10.3389/fpsyg.2022.972968. URL <https://www.frontiersin.org/journals/psychiatry/articles/10.3389/fpsyg.2022.972968>.
- Z. Wei, S. Alcauter, K. Jin, Z. Peng, and W. Gao. Graph theoretical analysis of sedation’s effect on whole brain functional system in school-aged children. *Brain connectivity*, 3, 01 2013. doi: 10.1089/brain.2012.0125.

- S. Wein, G. Deco, A. Tomé, M. Goldhacker, W. Malloni, M. Greenlee, and E. Lang. Brain connectivity studies on structure-function relationships: A short survey with an emphasis on machine learning. *Computational Intelligence and Neuroscience*, 2021:1–31, 05 2021a. doi: 10.1155/2021/5573740.
- S. Wein, W. Malloni, A. Tomé, S. Frank, G.-I. Henze, S. Wüst, M. Greenlee, and E. Lang. A graph neural network framework for causal inference in brain networks. *Scientific Reports*, 11, 04 2021b. doi: 10.1038/s41598-021-87411-8.
- S. Wein, M. Riebel, P. Seidel, L.-M. Brunner, V. Wagner, C. Nothdurfter, R. Rupprecht, and J. Schwarzbach. Local and global effects of sedation in resting-state fmri: a randomized, placebo-controlled comparison between etifoxine and alprazolam. *Neuropsychopharmacology*, 05 2024. doi: 10.1038/s41386-024-01884-5.
- L. Wu, Y. Zhang, F. Zhou, L. Gao, L. He, X. Zeng, and H. Gong. altered intra-and interregional synchronization in relapsing–remitting multiple sclerosis: a resting-state fmri study. *Neuropsychiatric Disease and Treatment*, pages 853–862, 2016.
- H. Yang, X.-Y. Long, Y. Yang, H. Yan, C.-Z. Zhu, X.-P. Zhou, Y.-F. Zang, and Q.-Y. Gong. Amplitude of low frequency fluctuation within visual areas revealed by resting-state functional MRI. *NeuroImage*, 36(1):144–152, 2007. ISSN 1053-8119. doi: <https://doi.org/10.1016/j.neuroimage.2007.01.054>.
- T. B. T. Yeo, F. M. Krienen, J. Sepulcre, M. R. Sabuncu, D. Lashkari, M. Hollinshead, J. L. Roffman, J. W. Smoller, L. Zöllei, J. R. Polimeni, B. Fischl, H. Liu, and R. L. Buckner. The organization of the human cerebral cortex estimated by intrinsic functional connectivity. *Journal of Neurophysiology*, 106(3):1125–1165, 2011. doi: 10.1152/jn.00338.2011. URL <https://doi.org/10.1152/jn.00338.2011>.
- Y.-F. Zang, T. Jiang, Y. Lu, Y. He, and L. Tian. Regional homogeneity approach to fmri data analysis. *NeuroImage*, 22:394–400, 06 2004. doi: 10.1016/j.neuroimage.2003.12.030.
- C. Zeng, L. Gu, Z. Liu, and S. Zhao. Review of deep learning approaches for the segmentation of multiple sclerosis lesions on brain mri. *Frontiers in Neuroinformatics*, 14, 2020. ISSN 1662-5196. doi: 10.3389/fninf.2020.610967. URL <https://www.frontiersin.org/journals/neuroinformatics/articles/10.3389/fninf.2020.610967>.
- Q.-H. Zou, C.-Z. Zhu, Y. Yang, X.-N. Zuo, X.-Y. Long, Q.-J. Cao, Y.-F. Wang, and Y.-F. Zang. An improved approach to detection of amplitude of low-frequency fluctuation (ALFF) for resting-state fMRI: Fractional ALFF. *Journal of Neuroscience Methods*, 172(1):137–141, 2008. ISSN 0165-0270. doi: <https://doi.org/10.1016/j.jneumeth.2008.04.012>. URL <https://www.sciencedirect.com/science/article/pii/S0165027008002458>.

Supplementary Information

Supplement I: Definitions

Resting-state fMRI metrics

Regional homogeneity We first investigate local connectivity, as defined by *regional homogeneity* (ReHo). Thereby ReHo characterizes the coherence of the BOLD signal within a local neighbourhood of voxels or vertices (Zang et al., 2004). In a neighbourhood containing N vertices, we computed ReHo as the average Pearson correlation coefficient r_{ij} between all pairs of timecourses i and j :

$$ReHo = \frac{\sum_{i \neq j} r_{ij}}{N(N-1)} \quad (1)$$

Low frequency fluctuations To further analyze changes in spectral characteristics of the BOLD signal, we study alterations in *fractional amplitude of low frequency fluctuation* (fALFF) values across the cortex (Zou et al., 2008). For each vertex i fALFF can be computed as the ratio of the power of the BOLD signal $S_i(t)$, after being filtered with a bandpass filter $h(t)$, to the power of the unfiltered signal $S_i(t)$:

$$fALFF = \sqrt{\frac{\sum_t (h(t) * S_i(t))^2}{\sum_t S_i(t)^2}} \quad (2)$$

Here $*$ denotes the convolution operation and t the temporal index. In our application we focused on the very low frequency range $0.01Hz - 0.05Hz$, which has shown to be characteristic for sedation effects observed in resting-state fMRI (Kiviniemi et al., 2000, 2003, 2005).

Functional connectivity efficiency *Functional connectivity* (FC) between two brain regions i and j was computed as the Pearson correlation coefficient r_{ij} between the averaged BOLD signals of these regions. When computing these correlation values between all N regions, a FC network can be characterized by an adjacency matrix $\mathbf{A} \in \mathbb{R}^{N \times N}$, whereby one entry a_{ij} of this matrix describes the FC strength between brain region i and j . The *shortest path length* d_{ij} between node i and node j in a network can be defined as the minimum number of edges traversed in an optimal path between those nodes. Based on this definition, the connection efficiency E_{ij} between two nodes i and j can be derived (Sporns, 2010):

$$E_{ij} = \frac{1}{d_{ij}} \quad (3)$$

The average FC efficiency (FCE) of a ROI i is thereby defined as:

$$E_i = \sum_j E_{ij} \quad (4)$$

Searchlight feature importance

To recover the importance of each input metric for decoding a specific brain state we used *Shapley additive explanations* (SHAP) (Lundberg and Lee, 2017). SHAP is an additive feature attribution method that allows to relate the contribution of input features to the prediction of a model. For a single input x the predictions of a model $f(x)$ are approximated by a linear relationship:

$$g(z') = \phi_0 + \sum_{i=1}^M \phi_i z'_i \quad (5)$$

with the explanation model $g(z')$ and coalition vector $z' \in \{0, 1\}^M$, indicating whether a feature is present or not, M the number of input features and Shapley values $\phi_i \in \mathbb{R}$ of feature i . These values can be approximated using different model specific and model agnostic methods described by Lundberg and Lee (Lundberg and Lee, 2017), whereby in our implementation we rely on the model-agnostic approach employing successive permutations of input features. We then compute the importance of an input feature i as the average of absolute Shapley values of all J test samples:

$$I_i = \frac{1}{J} \sum_{j=1}^J |\phi_i^{(j)}| \quad (6)$$

In our FuSL framework the input features of one SL decoder reflect the different rs-fMRI metrics m at different vertex locations v on the cortex. For each individual SL k we get in this manner an importance score $I_{mv}^{(k)}$, representing the contribution of metric m at vertex v in SL k . To obtain spatial maps that reflect the importance of a metric m across vertices v , we average over the importance scores of all SLs k that overlap in vertex v :

$$I_{mv} = \frac{1}{K} \sum_{k=1}^K I_{mv}^{(k)} \quad (7)$$

In a next step, to combine feature importance with the actual information content about a brain state at a specific location, we weight the importance I_{mv} with the decoding accuracy score s_v at each vertex v to compute the impact score defined as:

$$\Psi_{mv} = I_{mv} \cdot s_v \quad (8)$$

To additionally visualize, whether the values $X_{mv}^{(j)}$ of a metric m at vertex v are relatively increased or decreased between groups or treatments, we computed the average difference between samples p of group G_1 and samples q of group G_2 :

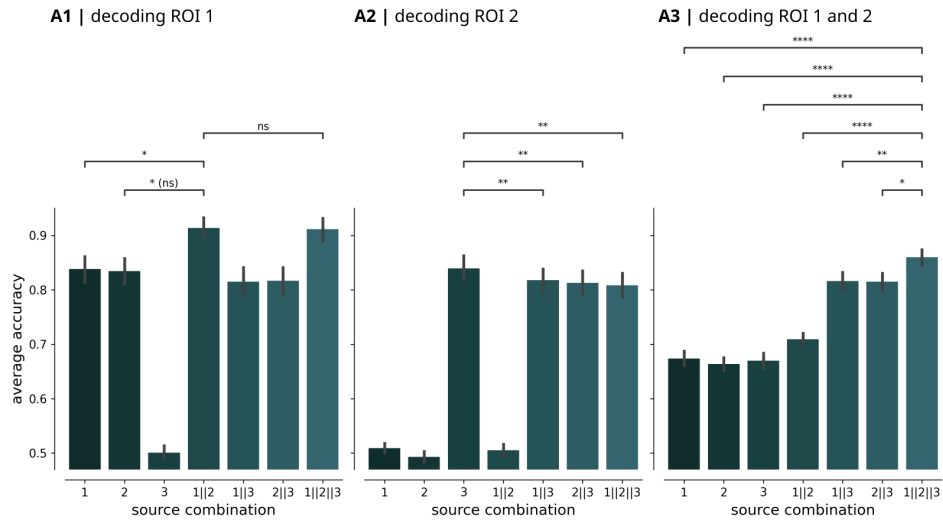
$$\Delta_{mv} = \frac{1}{P} \sum_{p \in G_1} X_{mv}^{(p)} - \frac{1}{Q} \sum_{q \in G_2} X_{mv}^{(q)} \quad (9)$$

Based on these differences we derived the feature-weighted impact of metric m at vertex v as:

$$\Phi_{mv} = \Psi_{mv} \cdot \Delta_{mv} \quad (10)$$

Supplement II: Supplementary figures and tables

A | $S/N = 2$



B | $S/N = 0.1$

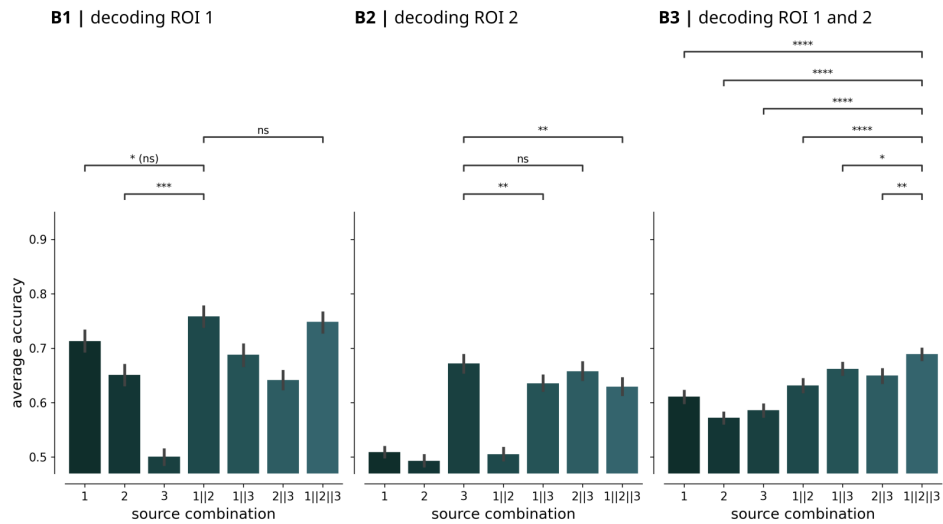


Figure S1: Decoding performance of FuSL in dependence of different noise levels. (A) Decoding accuracies when using sources with higher signal to noise ratios ($S/N = 2$). (A1) and (A2) show decoding accuracies for all combinations of sources in ROI 1 and 2 respectively, and (A3) the overall decoding accuracies averaged across ROI 1 and 2. (B) Decoding accuracies when using sources with lower signal to noise ratios ($S/N = 0.1$). Error bars represent 95% confidence intervals across folds. Significant differences of accuracies are indicated with: *: $p \leq 0.05$, **: $p \leq 0.01$, ***: $p \leq 0.001$, ****: $p \leq 0.0001$, ns: not significant, (ns): not significant after false discovery rate correction.

Table S1: P-values and effect sizes (Cohen's d) related to the comparison of decoding accuracies between ReHo||fALFF||FCE and all other respective combinations. All differences that remained significant after correcting for multiple comparisons are marked in bold font.

Comparison	p-value	effect size
ReHo fALFF FCE vs. ReHo	0.0005	0.765
ReHo fALFF FCE vs. FCE	0.0068	0.600
ReHo fALFF FCE vs. fALFF	0.0881	0.509
ReHo fALFF FCE vs. ReHo FCE	0.0078	0.505
ReHo fALFF FCE vs. ReHo fALFF	0.0318	0.225
ReHo fALFF FCE vs. ReHo fALFF	0.2267	0.028

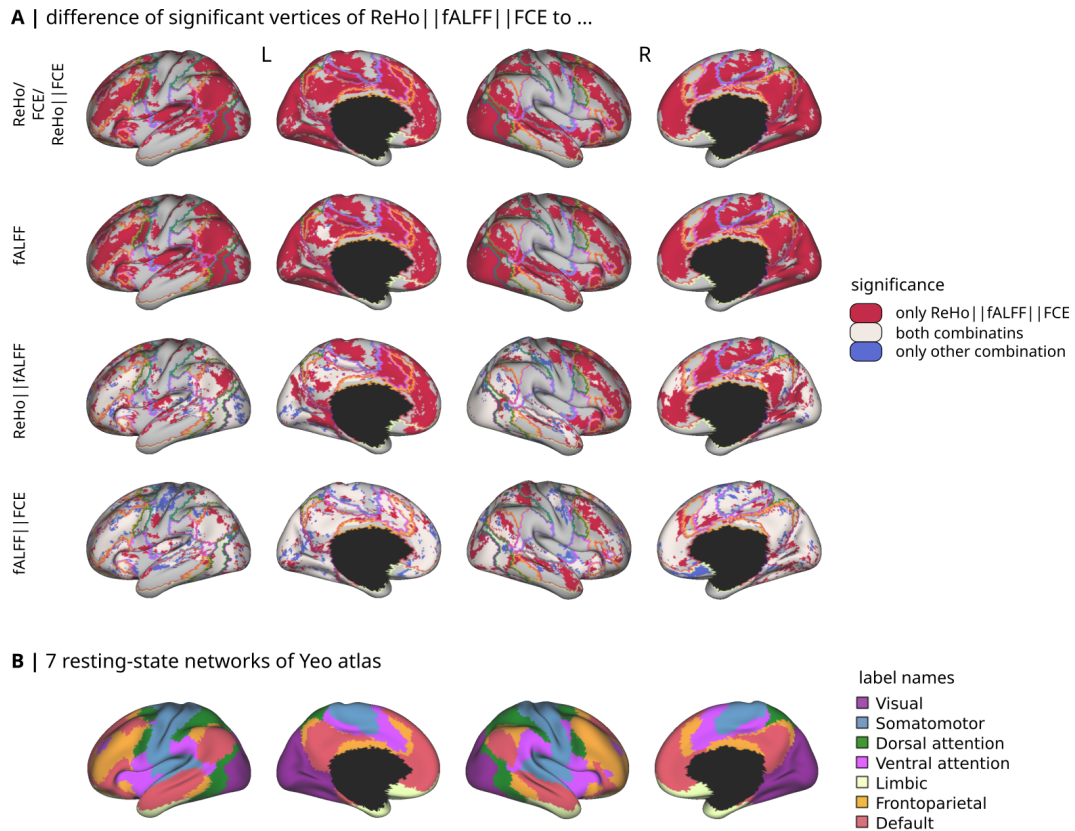
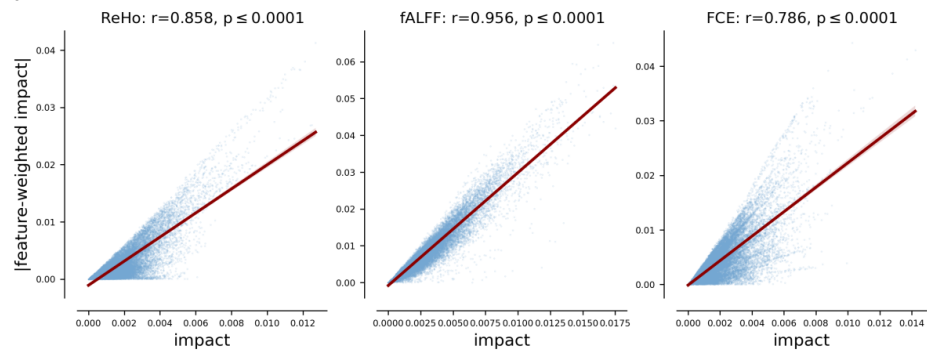
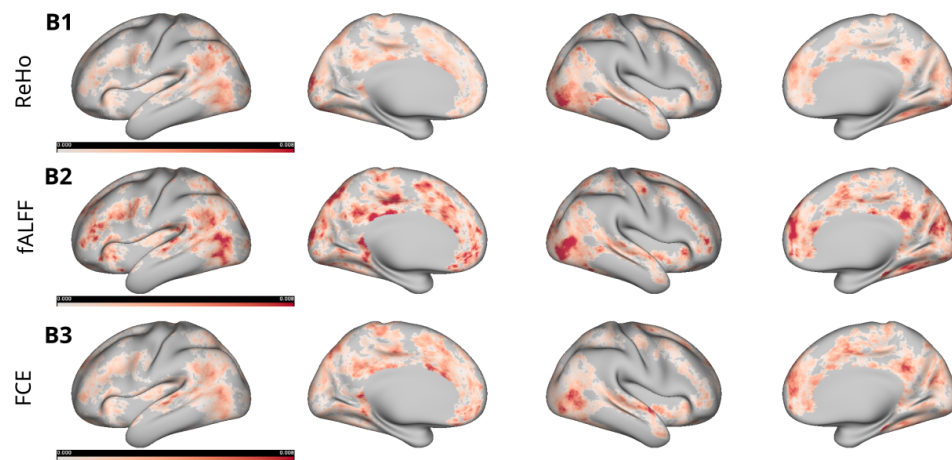


Figure S2: A comparison of significant vertices of combination ReHo||fALFF||FCE and all other combinations overlaid with resting-state networks defined by Yeo et al. (Yeo et al., 2011). (A) Locations where only ReHo||fALFF||FCE yields significant decoding accuracies are highlighted in red in the left (L) and right (R) cortex. Locations where both combinations can significantly decode are marked in white, and locations where only the other combination is able to decode are depicted in blue. (B) Displays the 7 resting-state networks defined by Yeo et al. (Yeo et al., 2011).

A | correlation



B | impact



C | feature-weighted impact

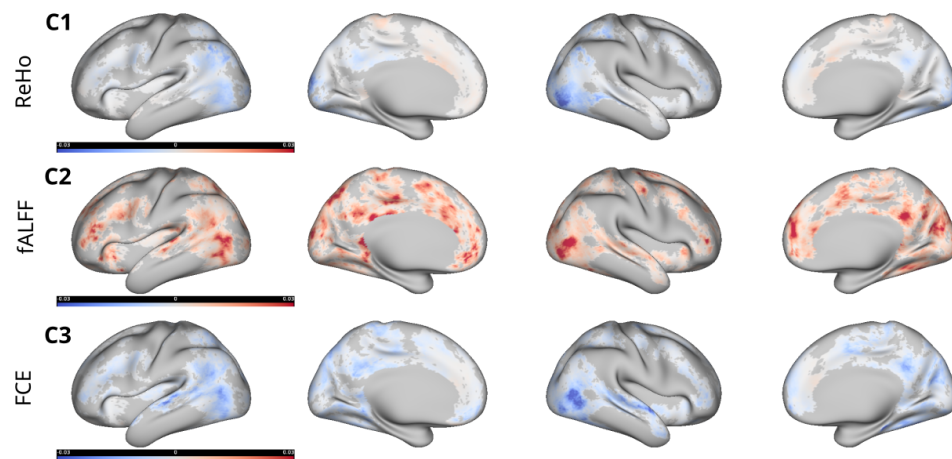
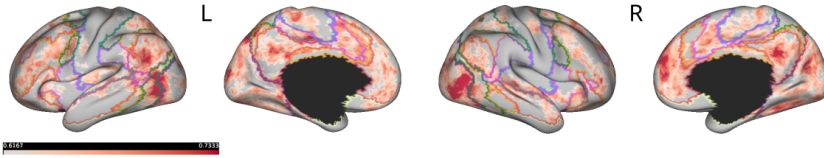
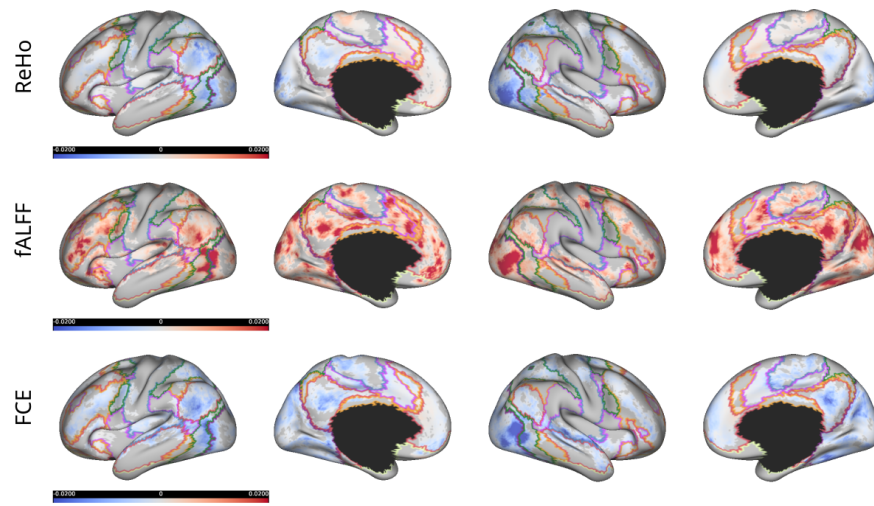


Figure S3: Comparison between impact and feature-weighted impact. (A) The impact and absolute feature-weighted impact values of all three rs-fMRI metrics are highly correlated across vertices. (B) Local impact of ReHo (B1), fALFF (B2) and FCE (B3) across the cortex. (C) Local feature-weighted impact of ReHo (B1), fALFF (B2) and FCE (B3) across the cortex.

A | decoding accuracy



B | feature-weighted impact



C | 7 resting-state networks of Yeo atlas

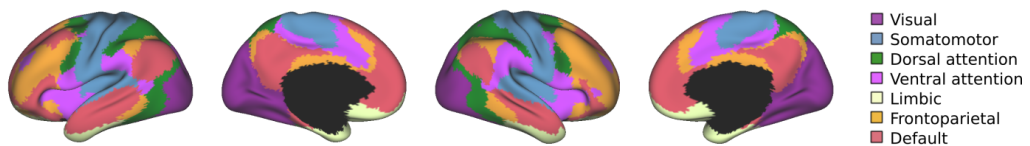


Figure S4: Decoding accuracy and feature-weighted impact of FuSL overlaid with resting-state networks defined by Yeo et al. (Yeo et al., 2011). (A) Decoding accuracy of FuSL across the cortex based on a combination of ReHo, fALFF and FCE. (B) The feature-weighted impact allows us to identify which brain areas are informative and important for the decoding and whether ReHo, fALFF and FCE are increased or decreased due to the treatment of alprazolam. (C) Displays the 7 resting-state networks defined by Yeo et al. (Yeo et al., 2011).